ELSEVIER

Catalysis Today 56 (2000) 211–220

CATALYSIS TODAY

www.elsevier.com/locate/cattod

Investigation of sol–gel methods for the synthesis of VPO membrane materials adapted to the partial oxidation of *n*-butane

D. Farrusseng, A. Julbe *, M. Lopez, C. Guizard

Laboratoire des Matériaux et Procédés Membranaires, UMR CNRS 5635, ENSCM, 8 Rue de l'Ecole Normale, 34 296 Montpellier Cedex 5, France

Abstract

The sol–gel process was used to prepare supported vanadium phosphate (VPO) membranes adapted to the mild oxidation of *n*-butane to maleic anhydride in a membrane reactor. Starting from a vanadium oxoalkoxide, two different sol–gel methods have been investigated: the colloidal route in aqueous media and the polymeric route in organic media. The membrane synthesis as well as the characteristics of the VPO precursors are described on the basis of the fundamental phenomena occurring during the sol–gel process. The VPO precursors and the derived catalysts were characterized through TGA, elemental analysis, LRS, XRD and N_2 adsorption–desorption. The polymeric route yielded an attractive hybrid organic–inorganic VPO precursor adapted to the synthesis of infiltrated VPO/α-Al_2O_3 composite membranes stable up to 500°C. N_2 permeation experiments were used to characterize the membranes after *n*-C_4H_{10} and O_2 heat-treatment cycles. Gravimetric analysis were useful to correlate the structural characteristics and permeation behavior of the VPO membranes after *n*-C_4H_{10} or O_2 treatments.

Keywords: Sol–gel process; VPO membrane; Membrane reactor

1. Introduction

The membrane reactor concept is of potential interest for increasing the selectivity of partial oxidation reaction by controlling the oxygen feeding and limiting the total combustion reactions [1]. An other possible function of a membrane reactor is to improve the contact between the reactants and the catalyst [1,2]. In the last case, the membrane does not need to be permselective but catalytically active, with a thickness and a porous texture adapted to the reaction kinetics. This work deals with the synthesis of a catalytically active membrane for the partial oxidation of *n*-butane to maleic anhydride (MA). The catalytic membrane material is based on VPO phases which are efficient catalysts for the foreseen reaction [3,4]. The VPO crystalline structures reported in the literature can be divided into two groups: the precursors which are hydrated VPO phases such as $VOPO_4{\cdot}nH_2O$ ($n = 1$–4) [5], $VOHPO_4{\cdot}nH_2O$ ($n = 0.5$–4) [6,7], $VOHPO_3{\cdot}1.5H_2O$ [8] and the pure catalytic phases αI, αII, β-, γ-, δ-$VOPO_4$ and $(VO)_2P_2O_7$ [9]. Each VPO phase leads to a specific MA selectivity [10] but the best catalysts are based on the vanadyl pyrophosphate $(VO)_2P_2O_7$ phase containing $VOPO_4$ microdomains [11,12]. A large number of methods have been reported in the literature for the synthesis of VPO catalysts [13]. Both the nature of the vanadium precursor (NH_4VO_3, V_2O_5, $VO(acac)_2$, VCl_3, etc.) [8,14–16]

* Corresponding author. Fax: +33-4-67144347.
E-mail address: ajulbe@cit.enscm.fr (A. Julbe).

0920-5861/00/$ – see front matter
PII: S0920-5861(99)00278-3

and of the synthesis media (aqueous or organic) [17] influence the structure, texture and consequently the catalytic performance of the VPO catalyst. VPO precursors are classically prepared by refluxing an aqueous suspension of V_2O_5 powder in a large excess of H_3PO_4 and with organic or inorganic additives [13,18]. These methods, based on the crystallization of VPO hydrated phases, are not well adapted to membrane synthesis. The sol–gel process is largely used for the preparation of thin films and ceramic membranes [19,20]. In 1986, Livage and co-workers [5] prepared sol–gel derived $VOPO_4{\cdot}2H_2O$ thin films on glass support at room temperature for electrochemical applications. The films were obtained from a sol prepared by acidification of an aqueous mixture of $NaVO_3$ and $NaPO_3$ through a proton exchange resin. This method is not simple to apply and leads to Na^+ impurities in the final oxide. On the contrary, sol–gel processing of molecular precursors appeared to us as a well-adapted method to prepare VPO supported membranes using vanadium alkoxides. These precursors allow the preparation of pure vanadium oxide films and the synthesis of binuclear compounds [21,22].

An original alkoxide ($VO(OCH(CH_3)CH_2OCH_3)_3$) was used as starting material to prepare membranes with a good thermo-mechanical stability and mainly consisting of the pyrophosphate $(VO)_2P_2O_7$ phase. The VPO phases derived from both colloidal and polymeric sols will be characterized and discussed. Finally, the redox properties and reactivity of the VPO membranes derived from the polymeric route will be studied through the evolution of the membrane N_2 permeance after *n*-C_4H_{10}/O_2 cycling at 500°C.

2. Experimental

2.1. Description of the membrane supports

Commercial alumina tubes (supplied by US Filter-SCT) were used as supports for the VPO membranes. The tubes are 15 cm long, enameled at each end on 2.5 cm, with internal/external diameters of 7/10 mm. The support structure is asymmetric with three different layers: an external layer 1.5 mm thick with 10 μm mean pore sizes, an intermediate layer 80 μm thick with 0.8 μm mean pore sizes and an internal layer 40 μm thick with 0.2 μm mean pore sizes. When necessary, a similar support was used with a γ-alumina top-layer (5 nm mean pore sizes).

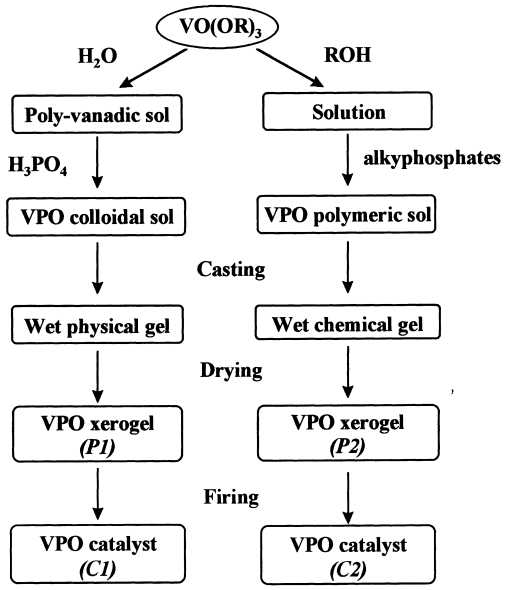

Fig. 1. Scheme for the preparation of VPO membranes: (left side) by the colloidal route; (right side) by the polymeric route.

2.2. VPO membranes and materials derived from the colloidal route P1 and C1

Polyvanadic acidic sols were formed under stirring by mixing 3.34 g of a home-made vanadium oxoalkoxide $VO(OCH(CH_3)CH_2OCH_3)_3$ with 100 ml of pure water (Fig. 1). After two days stirring at room temperature, a stoichiometric amount of 1.74M H_3PO_4 solution (Prolabo, 85%) was added and the mixture was heated 24 h at 60°C. The thixotropic sol was slip-cast in the inner part of the α-alumina support, dried in air at room temperature and then at 200°C. Because of the bad adhesion of the film on the α-alumina support, we rather used a commercial γ-alumina coated support. VPO membranes were obtained after a 4 h heat-treatment in N_2 (99.995% purity) at 750°C. The corresponding unsupported materials were prepared by casting the sol on a Teflon foil and scrapping-off after drying. The dried and fired materials are called, respectively, P1 (precursor) and C1 (catalyst) in the following sections.

2.3. VPO membranes and materials derived from the polymeric route P2 and C2

The VPO polymeric sol was prepared from a stoichiometric mixture (1:1) of di-*n*-propylphosphate (Strem-Chemicals) and of the home made oxoalkoxide $VO(OCH(CH_3)CH_2OCH_3)_3$ in 1-methoxy 2-propanol (Aldrich, 98%) (Fig. 1). The reaction mixture was refluxed during 16 h, yielding a blue solution which was concentrated under low pressure in order to increase its viscosity. The sol deposition inside the α-Al_2O_3 tube leads to a total infiltration. The following sequence: sol impregnation in the support — air drying — firing 4 h at 650°C in air (heating rate 2°C min^{-1}) — was repeated typically five times, until the tube reached a stable weight. The unsupported materials were prepared by casting the sol on a Teflon foil; the dried and fired materials are called, respectively, P2 (precursor) and C2 (catalyst) in the following sections.

2.4. Characterizations

The chemical compositions of the VPO precursors and catalysts were determined by elemental and thermogravimetric analysis (Setaram TG85). The VPO phases were characterized by laser Raman spectroscopy (LRS) and X-ray diffraction (Cu Kα radiation, curved detector Inel CPS120). Both LRS and XRD are commonly used for the characterization of VPO catalysts [30]. The LRS apparatus (Labram 1B), equipped with a camera ($\times$100), was useful to study the structural homogeneity of the samples. Field Emission Scanning Electron Microscopy (Hitachi S-4500), N_2 adsorption–desorption (Micromeritics ASAP2000) and Hg porosimetry (Micromeritics AutoporeII 9220) were used for the morphological and textural characterizations of the membranes. The specific surface area of the samples were calculated with the BET method from the N_2 adsorption isotherm.

The N_2 permeance of the VPO membranes (equipped with graphite o-rings) was measured with a home-made apparatus at room temperature as a function of the transmembrane pressure ΔP ($\Delta P = P_{int} - P_{ext}$). The transmembrane pressure was varied from 0.5 to 2.5 bar and the external pressure was the atmospheric pressure. The N_2 flow at the outlet of the reactor was measured with a bubble-flow meter.

The redox properties of the membranes derived from the polymeric route were studied by both gravimetric and N_2 permeance measurements. The weight variation studies of a tubular membrane sample submitted to *n*-C_4H_{10} or O_2 atmosphere at 500°C were carried out in a TG balance. After every 90 min, the atmosphere was changed from pure *n*-C_4H_{10} to O_2 (flow rate 40 ml min^{-1}). Before each change in the atmosphere, the system was purged with Ar. The sample weight was continuously recorded during three butane/oxygen cycles. Concurrently, the N_2 permeance of the VPO membrane was measured (at room temperature with $\Delta P = 0.5$ bar) after each corresponding *n*-C_4H_{10} or O_2 (1 h) treatment at 500°C.

3. Results and discussion

3.1. VPO membranes derived from the colloidal route

3.1.1. From the molecular precursors to the sol

In water media, the vanadium alkoxide was rapidly and fully hydrolyzed leading to the precipitation of the hydroxide which was then modified by the nucleophilic addition of two water molecules [21]. The condensation of the neutral species $[VO(OH)_3(OH_2)_2]^0$ occurred spontaneously in specific directions leading to ribbon-like polymeric species as confirmed in [20]. The addition of H_3PO_4 and subsequent heating favored the V–O–P condensation in the sol. Upon aging, the sol viscosity increased, leading to a physical gel in a few days. The rheological properties of this type of sol is typically adapted to slip-casting on porous supports.

3.1.2. From the sol to the gelled film P1

The ribbon-like texture of the sol, containing colloidal particles larger than 500 nm, prevents sol penetration in the porous support. The thickness of the gelled films can be controlled between 0.1 and 2 μm by varying the sol aging period and the sol/support contact time. Thin gelled films were obtained within a few seconds by contact between the support and a fresh sol, whereas thicker films were obtained within several minutes by contact between the support and aged sol. During the drying step, both the released alcohol and the water evaporated, leading to dark-red

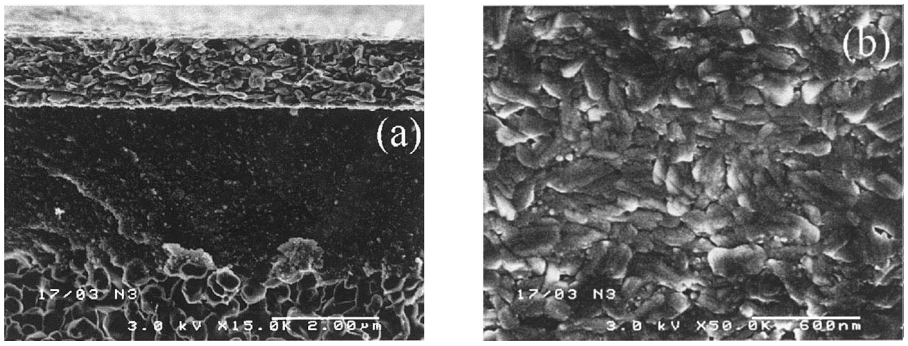

Fig. 2. VPO ceramic membrane derived from the colloidal route on γ-alumina support: (a) cross-sectional view; (b) surface view.

xerogel VPO films. This membrane material (P1) has been characterized by XRD (*d*-spacing = 7.47 Å) and LRS as being $VOPO_4 \cdot 2H_2O$. The VPO layered structure provides a host structure for two guest water molecules [23]. Elemental analysis results (2.0 wt.% H, 24.8 wt.% V and 14.9 wt.% P) confirms the dihydrate phase for P1.

3.1.3. From the gelled film to the ceramic membrane

SEM observations of the fired supported films showed that the method leads to crack-free layers, with an homogeneous texture and a constant thickness of typically 1.5 μm along the tube (Fig. 2). The weight of the VPO catalytic film on a γ-Al_2O_3 support is about 20 mg. The grains are elongated with sizes in the range 100–400 nm, thus leading to a meso/macroporous structure. In good agreement with these observations, N_2 adsorption–desorption studies showed a low porous volume ($\approx 0.02\ cc\ g^{-1}$) and a low specific surface area ($S_{BET} < 5\ m^2\ g^{-1}$) for this membrane material.

3.2. VPO membranes derived from the polymeric route

3.2.1. From the molecular precursors in solution to the sol

The strong electrophilic character of the vanadium atom in the starting alkoxide favors nucleophilic substitution reactions in which alkoxy groups are displaced by the phosphate groups (Fig. 3). The substitution is also favored by the low steric hindrance of the alkoxy groups (secondary alcohol) [24]. Both the vanadium and phosphorous precursors contain several reactive groups which lead to a progressive polymerization of the formed species. This polymerization was favored by the increasing electrophilic character of the vanadium atoms when linked to phosphate groups (inducting effect). This heteronuclear polymerization controls the P/V ratio in the VPO species (chains) formed at the sol stage. These species still contain unreacted organic groups which allowed a good solubility in an alcoholic solvent [25]. If phosphoric acid $PO(OH)_3$ is used instead of alkylphosphates for this reaction, the resulting tridimensional VOP network without organic groups, should lead to a rapid precipitation due to unfavorable interactions between the organic solvent and the mineral polymer [24]. When refluxed, the sol turns blue, due to a reduction of V(V)

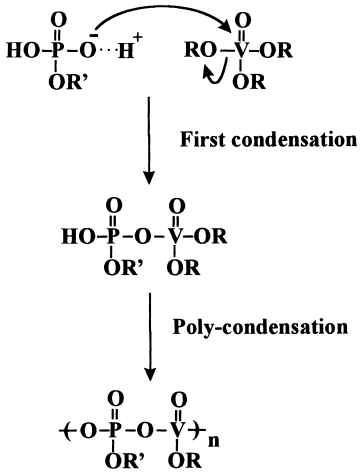

Fig. 3. Suggested scheme for the hetero-nuclear polymerisation.

to V(IV) species in alcoholic media [26,27]. To a great extent this reduction is favored by the high refluxing temperature (119°C) [28].

3.2.2. From the sol to the gelled film P2

In order to adapt the sol viscosity to casting in tubular porous supports, the sol concentration was increased by solvent evaporation under reduced pressure. After infiltration of the sol in the support, the solvent was slowly evaporated during the drying step in air. When the sol was deposited on a Teflon foil, the resulting blue film (P2) showed plastic properties attributed to the presence of unreacted organic groups attached to the V–O–P network. The proportion of the organic part in this hybrid organic–inorganic VPO dry gel (P2) was estimated to about 30% from TG analysis (29.6 wt.% loss between 180 and 500°C). The hybrid VPO gel was fully amorphous by XRD. These results differ from those reported in the literature for a series of VPO based compounds with alkyl chains linked to the phosphorous atoms. In these compounds, an organization of the organic part between the VPO layers was shown to lead to microcrystallites [29].

3.2.3. From the gelled film to the ceramic membrane

SEM observations of the asymmetric support obtained after sol deposition and firing at 650°C in air, revealed that the VPO material was infiltrated in the pores of the support (Fig. 4). The pores of the internal and intermediate layers seem almost completely filled with the VPO material, whereas the alumina grains of the external layer are covered with VPO. Hg porosimetry confirmed these SEM observations: after synthesis, 0.2 and 0.8 μm pores disappeared and the volume of the 10 μm pores was decreased by 10% (Fig. 5). The N_2 adsorption–desorption isotherms of the VPO/α-Al_2O_3 composite membrane are typical of a macroporous material, with a small mesoporous contribution (Fig. 6). The specific surface area is very low ($S < 5\,m^2\,g^{-1}$). Similar isotherms were obtained with the unsupported VPO material (Fig. 6). All these results suggest the formation of a compact composite VPO/α-Al_2O_3 membrane with a thickness of about 60 μm and with a very low pore volume mainly due to macropores. The quantity of VPO catalyst inserted in the support is typically 650 mg (i.e. 30 times higher than that in the colloidal route). This higher quantity of catalyst should increase the reactant conversion during the catalytic reaction.

3.3. Characterizations of the VPO phases in the membrane materials C1 and C2

3.3.1. Membrane materials derived from the colloidal route C1

Both the XRD pattern (Fig. 7) and the Raman spectra (Fig. 8) of the VPO phase obtained after the firing treatment at 750°C in N_2, were consistent with pure $(VO)_2P_2O_7$ [30] which is the best catalytic VPO phase for the foreseen reaction. The main XRD lines are at $2\theta = 22.97°$, 28.46° and 29.92°, and the intense LRS peaks are at 924, 935, 1187, 270 and 255 cm^{-1}. During the N_2 heat-treatment, the orthophosphate structure of the P1 precursor transformed to a pyrophosphate structure through a reduction from V(V) to V(IV). This phase transformation needs a high temperature (up to 750°C) and a flow of N_2 with a high purity grade [31]. Such a high temperature favors grain growth and contributes to lower the specific surface area of the final catalyst (C1).

3.3.2. Membrane materials derived from the polymeric route C2

Both the XRD pattern (Fig. 9) and the Raman spectra (Fig. 10) of the final catalyst (C2) derived from the polymeric route at 650°C in air, revealed a mixture of several VPO phases [30]. The major identified phase, corresponding to at least 50% of the catalyst, is $(VO)_2P_2O_7$ as revealed by the XRD peaks at $2\theta = 22.96°$, 28.47° and 29.95°. The other VPO phases were more difficult to identify because of peaks overlapping. We detected anyway the presence of γ-$VOPO_4$ (18.16°, 21.41°, 28.79°), δ-$VOPO_4$ (19.53°, 22.16°, 4.21°) and β-$VOPO_4$ (17.14°, 19.35°, 26.24°, 29.95°). The αII-$VOPO_4$ phase was not detected. These results were confirmed by LRS data showing strong absorption bands characteristic of γ-$VOPO_4$ (1038, 655, 599, 392 cm^{-1}), δ-$VOPO_4$ (1040, 1019 cm^{-1}) and β-$VOPO_4$ (988, 1073, 895, 433, 997, 367, 320, 295 cm^{-1}). Because the two strong and sharp bands characteristic of $(VO)_2P_2O_7$ (924, 935 cm^{-1}) overlapped with the broad band of δ-$VOPO_4$ at 1040 cm^{-1}, only a shoulder at 927 cm^{-1} was observed. We have to note that all these phases

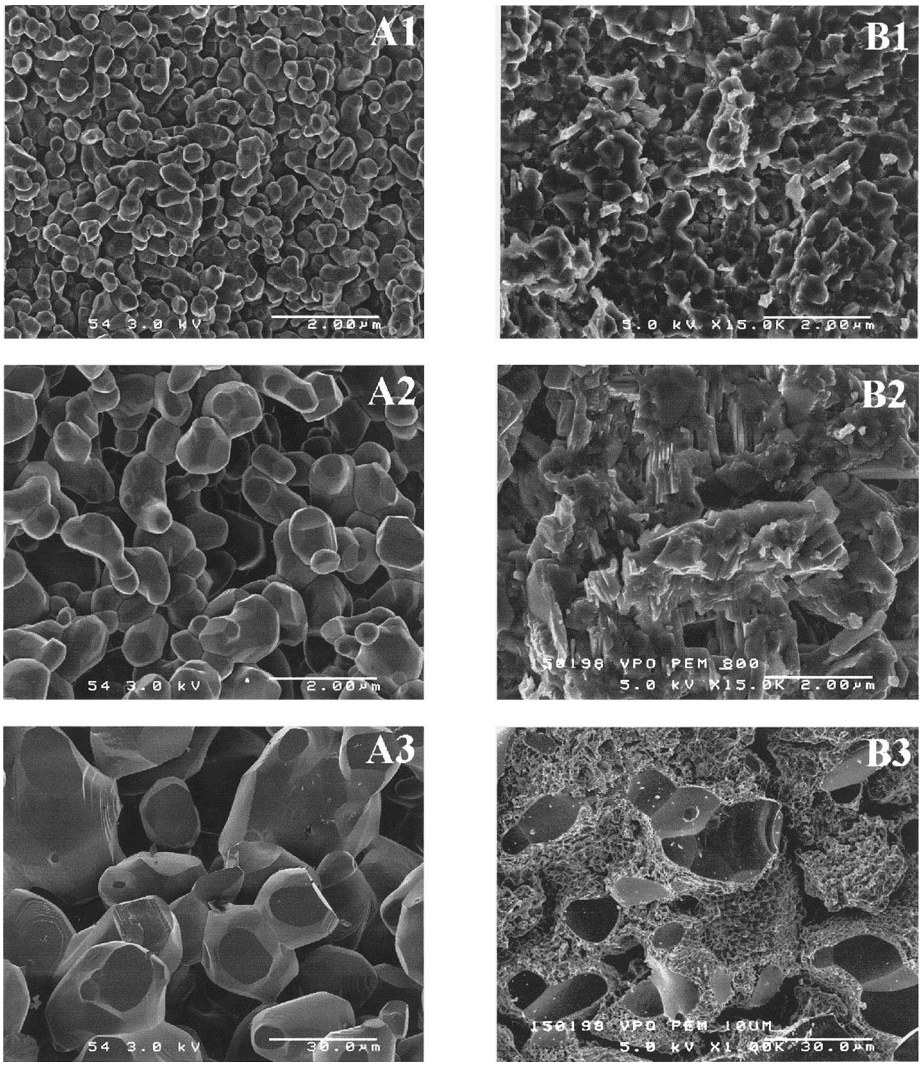

Fig. 4. Cross-sectional view of the three layers of the asymmetric support (A) before and (B) after the VPO impregnation by the polymeric route: (1) internal layer; (2) intermediate layer; (3) external layer.

were detected by an LRS on a 1 mm^2 surface, this means that the phases are mixed on a micrometer scale. All the above results suggest that the catalyst (C2) is a mixture of VPO microdomains mainly consisting of $(VO)_2P_2O_7$ and of a lower quantity of γ-, δ- and β-$VOPO_4$ phases. It is now well established that such a dispersion of $VOPO_4$ phases in a $(VO)_2P_2O_7$ matrix acts as a dopant and should lead to a highly selective catalyst [10], [32]. One can note that although the P2 precursor was thermally treated in an oxidizing atmosphere, a large proportion of V(IV) was obtained in the final C2 catalyst. This is attributed to the great quantity of V(IV) in the blue precursor (P2), but also to the presence of organic products graft on the inorganic network. The V(IV)/V(V) ratio in the final catalyst should be increased by firing the precursor at a temperature lower than 650°C and/or by using a reducing atmosphere. The firing treatment of the membrane was fixed at 650°C in order to ensure a good thermal stability for the membrane during

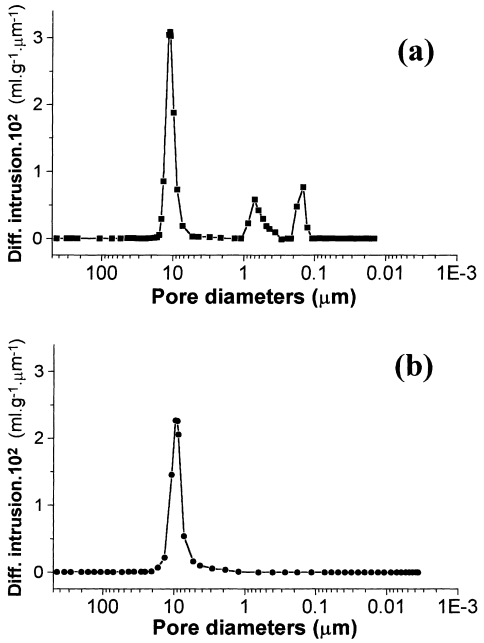

Fig. 5. Pore-size distributions obtained by Hg porosimetry analysis of the support: (a) before and (b) after VPO synthesis by the polymeric route.

the partial oxidation reactions usually carried out at 380–450°C.

3.4. N_2 permeance of the VPO membranes

When VPO membranes were prepared by deposition of a colloidal sol on top of a γ-Al_2O_3 supporting layer, it was not possible to observe any modification of the support permeance after the VPO deposition. The thin VPO layer did not modify the transport resistance of the mesoporous supporting layer because of its macroporous structure.

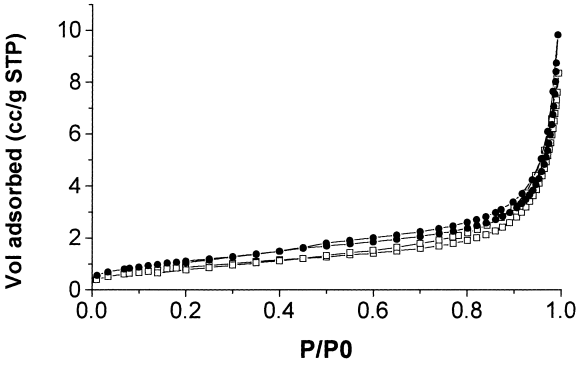

Fig. 6. N_2 adsorption–desorption isotherms of the VPO infiltrated membrane derived from the polymeric route (□) and of the corresponding VPO unsupported material (●). The adsorbed volumes are reported per gram of catalyst in both cases.

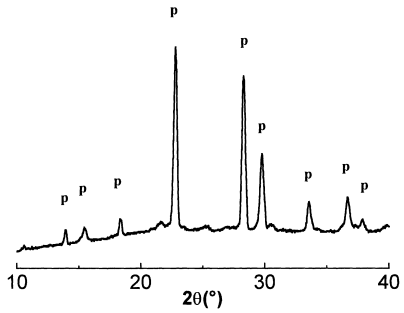

Fig. 7. XRD pattern of C1, derived from the colloidal route and fired at 750°C in N_2 (p indicates the $(VO)_2P_2O_7$ phase).

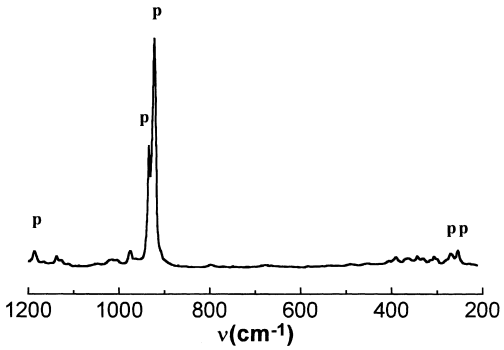

Fig. 8. Laser Raman spectra of C1, derived from the colloidal route and fired at 750°C in N_2 (p indicates the $(VO)_2P_2O_7$ phase).

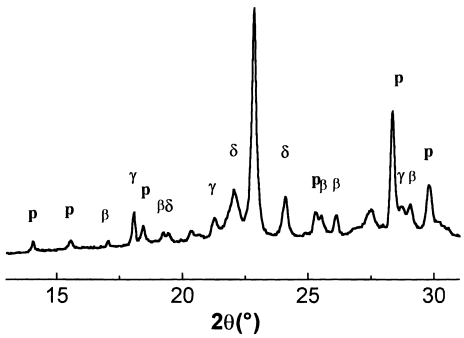

Fig. 9. XRD pattern of C2, derived from the polymeric route and fired at 650°C in air (p indicates the $(VO)_2P_2O_7$ phase and β, δ, γ correspond to $VOPO_4$ phases).

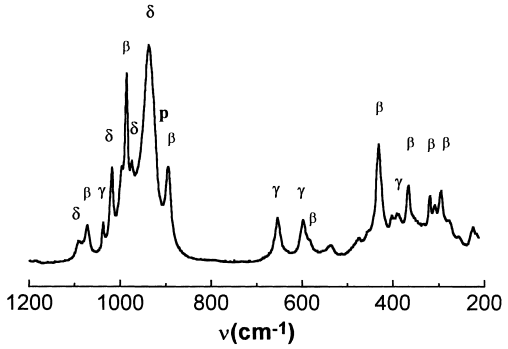

Fig. 10. Laser Raman spectra of C2, derived from the polymeric route and fired at 650°C in air (p indicates the $(VO)_2P_2O_7$ phase and β, δ, γ correspond to $VOPO_4$ phases).

In the case of VPO membranes derived from polymeric sols and infiltrated in the α-Al_2O_3 macroporous support, the N_2 permeance (P_{N_2}) was a linear function of the transmembrane pressure (ΔP): $P_{N_2} = (7.12 + 1.60 \cdot \Delta P)10^{-8}$ mol Pa^{-1} s^{-1} m^{-2}. Such a pressure dependence is typical of a viscous flow gas transport mechanism and confirms the macroporous structure of the membrane (presence of pores >50 nm). On the other hand the low measured permeance values are indicative of a low membrane porosity.

3.5. Influence of n-C_4H_{10} and O_2 treatments on the characteristics of the membranes derived from the polymeric route

Fig. 11 shows the evolution of P_{N_2} at room temperature after successive heat-treatments of the

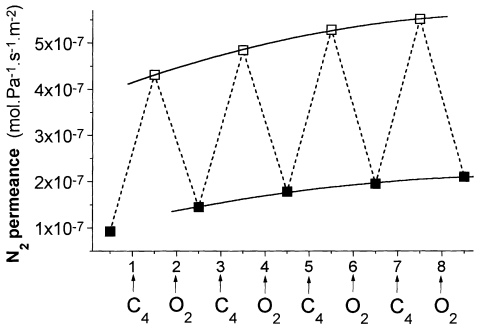

Fig. 11. Evolution of the N_2 permeance, measured at room temperature, through a VPO/α-Al_2O_3 membrane derived from the polymeric route after successive heat treatments at 500°C in pure n-C_4H_{10} or O_2: (□) reduced membrane; (■) oxidized membrane.

VPO/α-Al_2O_3 composite membrane at 500°C with pure n-C_4H_{10} and then with O_2. The initial permeance value ($P_{N_2} := 0.8 \times 10^{-7}$ mol Pa^{-1} s^{-1} m^{-2}) was measured with the fresh membrane obtained after firing at 650°C in air. After the first treatment with n-C_4H_{10} at 500°C, P_{N_2} at room temperature increased up to 4.3×10^{-7} and then decreased again down to 1.4×10^{-7} after the O_2 treatment at 500°C. Such permeation behavior was reproduced during four successive n-C_4H_{10}/O_2 cycles. It can be observed in Fig. 11 that the P_{N_2} values measured after each oxidative or reducing treatment tend to increase and reach a stable value after four cycles. Such heating/cooling cycles at 500°C under n-C_4H_{10} or O_2 helps to stabilize the membrane. P_{N_2} are higher after treating the membrane with n-C_4H_{10} than after O_2 treatments. The ratio of permeances: P_{N_2}(after n-C_4H_{10})/P_{N_2}(after O_2) stabilizes to around 2.7 for the two last cycles. Such results can be explained neither by coke deposition, nor by a specific N_2 adsorption phenomenon on the modified VPO grains surface. In fact, a modification of the membrane porous texture during cycling seems to be responsible for these results. Due to the very low membrane porous volume it has not been possible to evidence any textural modification by N_2 adsorption–desorption or Hg porosimetry on membrane samples before and after n-C_4H_{10} treatment at 500°C.

In order to study the membrane modification, we performed a gravimetric analysis on a membrane sample submitted to n-C_4H_{10}/O_2 cycling at 500°C. The sample was initially heat-treated in the TG cell at 800°C in O_2 in order to totally oxidize the VPO catalyst and to obtain only V(V) species. This oxidation should theoretically lead to a $VOPO_4$/α-Al_2O_3 composite membrane (considered as initial zero weight reference). Results reported in Fig. 12 reveal the important variation of the sample weight during the n-C_4H_{10}/O_2 cycling experiments. When submitted to n-C_4H_{10} the sample weight loss was −4.2% after 3.5 min and reached −8.5% after 20 min. This weight loss was followed by a slow weight increase which reaches +0.5% and lead to a total weight loss of −8% for the sample after 90 min. When the atmosphere was changed to O_2, the sample weight rapidly increased and reached the initial weight after 20 min. Upon time, we also noticed a slow but continuous weight increase which reached +0.4% after

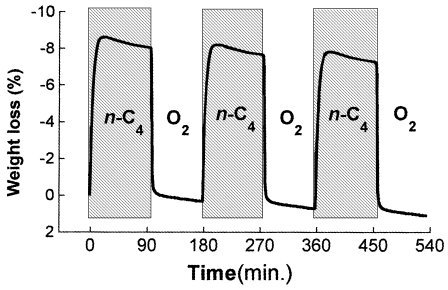

Fig. 12. Weight evolution of a VPO/α-Al_2O_3 membrane sample (derived from the polymeric route) during *n*-C_4H_{10}/O_2 cycling at 500°C.

90 min. These phenomenon have been reproduced during three *n*-C_4H_{10}/O_2 cycles. The TG study was also performed on unsupported VPO material and results were in good agreement with those of Bordes and Courtine [31] obtained with 1-butene and O_2 at 450°C, however, three main differences were noticed between the VPO/α-Al_2O_3 composite membrane and the unsupported VPO sample. First of all, the weight gain and loss were entirely reversible with the membrane but not with the powder. Furthermore the slight weight increase observed after 20 min under *n*-C_4H_{10} was only observed with the membrane and might correspond to a coke deposition. Finally, the weight gain and loss values (+/−8.5%) were higher for the membrane than for the unsupported material (+/−4.9%). This last value fits with the reduction from $V^{5+}OPO_4$ to $V^{4+}OPO_{3.5}$ (by the loss of 1/4 O_2 from the oxide network) although a weight loss of −8.5% should rather correspond to the formation of V^{3+} containing species (theoretical weight loss = −9.9% for the reduction from $V^{5+}OPO_4$ to $V^{3+}OPO_3$). The observed differences between the VPO/α-Al_2O_3 membrane and the VPO powder might be due to a chemical modification of the VPO crystals by the alumina from the support. Such an interaction which should modify the composition, structure and performance of the VPO catalyst is currently under investigation.

The permeance results showed that P_{N_2} was higher when the VPO/α-Al_2O_3 membrane was reduced, and lower when it was oxidized. During the reduction in *n*-C_4H_{10} we can suppose that the important weight loss due to the departure of oxygen atoms from the VPO catalyst decreased the grain sizes and consequently increased the membrane pore sizes, porosity and permeance. Under O_2 atmosphere, the oxygen lattice was restored and the VPO grain volume was increased, leading to a decrease in the membrane pore sizes, porosity and permeance.

4. Conclusions

Starting from a home-made vanadium oxoalkoxide, the sol–gel process was used in aqueous or organic media to prepare original VPO membranes supported in/on commercial α-Al_2O_3 tubular supports. The colloidal route leads to $VOPO_4 \cdot 2H_2O$ dried coatings and to thin $(VO)_2P_2O_7$ top layers after a heat-treatment at 750°C under N_2. This type of membrane is of low interest for membrane reactor application because it contains a low quantity of catalyst which does not provide any barrier effect. The polymeric route was found to be more attractive because V–O–P bonds form at the sol stage, the sol viscosity can be controlled and it is possible to prepare infiltrated membranes. The method leads first to an hybrid organic–inorganic VPO gel which mainly contains V^{4+} species. After firing in air, 60 μm thick VPO/α-Al_2O_3 composite membranes were obtained. In spite of the low specific surface area of the VPO catalyst, several characteristics of the membrane are attractive and in good keeping with our objectives: reproducibility of the synthesis, thermal stability at 500°C, high catalyst loading in the support, $(VO)_2P_2O_7$ in the fresh membrane material and reversible redox reactivity of the membrane with *n*-C_4H_{10} and O_2. The membrane permeance was stabilized after several heating–cooling cycles up to 500°C and under *n*-C_4H_{10} or O_2 atmosphere. The next step will be to study the VPO membrane performance as a contactor/separator for the partial oxidation of *n*-butane to maleic anhydride.

Acknowledgements

We gratefully acknowledge financial support by the European Commission (Brite EuRam program BRPR CT 95-0046). The authors express their sincere thanks to N. Hovnanian, L. Albaric and G. Volle (LMPM-Montpellier) for the vanadium oxoalkoxide synthesis and to J.C. Volta (Institut de Recherches sur la Catalyse, CNRS, Villeurbanne) for useful and motivating discussions on VPO catalysts.

References

[1] M.P. Harold, C. Lee, A.J. Burggraaf, K. Keiser, V.T. Zaspalis, R.S.A. De Lange, MRS Bull. 9 (1994) 44.
[2] A. Julbe, D. Farrusseng, C. Guizard, in: P. Vincenzini (Ed.), Proceedings of the Ninth CIMTEC World Ceramic Congress, 14–19 June 1998, Techna srl, Firenze, Italy.
[3] G. Centi, F. Trifiro, J.R. Ebner, V.M. Franchetti, Chem. Rev. 88 (1988) 55.
[4] F. Cavani, F. Trifiro, Appl. Catal. A 88 (1992) 15.
[5] C. R′Kha, M.T. Vandenborre, J. Livage, J. Solid State Chem. 63 (1986) 202.
[6] P. Amoros, R. Ibanez, A. Beltran, A. Fuertes, P. Gomez-Romero, E. Hernandez, J. Rodriguez-Carvajal, Chem. Mater. 3 (1991) 407.
[7] D. Beltran-Porter, A. Beltran-Porter, P. Amoros, R. Ibanez, E. Martinez, A. le Bail, G. Ferey, G. Villeneuve, Eur. J. Solid State Inorg. Chem. 28 (1991) 131.
[8] V.V. Guliants, J.B. Benziger, S. Sundaresen, J. Catal. 156 (1995) 298.
[9] E. Bordes, Catal. Today 3 (1988) 163.
[10] Y.J. Zhang-Lin, M. Forissier, R.P. Sneeden, J.C. Vedrine, J.C. Volta, J. Catal. 145 (1994) 267.
[11] J.C. Volta, Catal. Today 32 (1996) 29.
[12] M. Abon, K.E. Bere, A. Tuel, P. Delichere, J. Catal. 156 (1995) 28.
[13] B.K. Hodnet, Catal. Rev. Sci. Eng. 27 (1985) 373.
[14] E. Bordes, Catal. Today 1 (1987) 499.
[15] N. Guilhaume, M. Roullet, G. Pajonk, B. Grzybowska, J.C. Volta, Stud. Surf. Sci. Catal. 72 (1992) 255.
[16] J. Vedrine, J.C. Volta, J. Catal. 128 (1991) 248.
[17] F. Cavani, A. Colombo, F. Trifiro, P. Vazquez, Prepr. Am. Chem. Soc. Div. Pet. Chem. 40 (1995) 12.
[18] G. Hutchings, R. Olier, M.T. Sananés, J.C. Volta, Stud. Surf. Sci. Catal. 82 (1994) 213.
[19] P. Chanaud, A. Julbe, A. Larbot, C. Guizard, L. Cot, H. Borges, A. Giroir Fendler, C. Mirodatos, Catal. Today 25 (1995) 225.
[20] S.I. Hong, J.H. Jung, Appl. Catal. A 156 (1997) 239.
[21] J. Livage, Solid State Ionics 86–88 (1996) 935.
[22] S. Lu, L. Hou, F. Gan, Adv. Mater. 9 (1997) 244.
[23] F. Benabelouahad, J.C. Volta, R. Olier, J. Catal. 148 (1994) 334.
[24] S.A. Ennaciri, C. R′Kha, P. Bardoux, J. Livage, Eur. J. Solid State Inorg. Chem. 30 (1993) 227.
[25] J. Livage, M.T. Bardoux, M.T. Vandenborre, C. Schmutz, F. Taulelle, J. Non-Cryst. Solids 147/148 (1992) 18.
[26] L.M. Cornaglia, C.A. Sanchez, E.A. Lombardo, Appl. Catal. A 95 (1993) 117.
[27] I.J. Ellison, G.J. Hutchings, M.T. Sananes, J.C. Volta, J. Chem. Soc., Chem. Commun. (1994) 1093.
[28] J.W. Johnson, D.C. Johnston, A.J. Jacobson, J.F. Brody, J. Am. Chem. Soc. 106 (1984) 8123.
[29] J.W. Johnson, A.J. Jacobson, M.B. Wayne, S.E. Rosenthal, J.F. Brody, J.T. Lewandowski, J. Am. Chem. Soc. 111 (1989) 381.
[30] F. Benabdelouahab, R. Olier, N. Guilhaume, F. Lefebvre, J.C. Volta, J. Catal. 134 (1992) 151.
[31] E. Bordes, P. Courtine, J. Catal. 57 (1979) 236.
[32] F. Rouvet, J.M. Hermann, J.C. Volta, J. Chem. Soc. Faraday Trans. 90 (1994) 1441.